Supporting Information

Redox-dependent conformational changes of a proximal [4Fe-4S] cluster in Hyb-type [NiFe]-hydrogenase to protect the active site from O_2

Noor Dina Muhd Noor[‡,a,b,d], Hiroaki Matsuura[‡,a,d], Koji Nishikawa[‡,a,c,d], Hulin Tai[‡d,e], Shun Hirota[d,e], Jaehyun Kim[a], Jiyoung Kang[a,f], Masaru Tateno[a], Ki-Seok Yoon[g,h], Seiji Ogo[g,h], Shintaro Kubota[a,i], Yasuhito Shomura[d,j] and Yoshiki Higuchi[*,a,c,d]

[a] Department of Life Science, Graduate School of Life Science, University of Hyogo, 3-2-1 Koto, Kamigori-cho, Ako-gun, Hyogo 678-1297, Japan
[b] Present address: Enzyme & Microbial Technology Research Centre (EMTech),Faculty of Biotechnology & Biomolecular Sciences, University Putra Malaysia, 43400 UPM Serdang, Selangor, Malaysia.
[c] RIKEN SPring-8 Center, 1-1-1 Koto, Sayo-gun, Sayo-cho, Hyogo 679-5148, Japan
[d] Core Research for Evolutional Science and Technology (CREST), Japan Science and Technology Agency (JST), Kawaguchi Center Building, 4-1-8 Honcho, Kawaguchi-shi, Saitama 332-0012, Japan
[e] Division of Materials Science, Graduate School of Science and Technology, Nara Institute of Science and Technology, 8916-5 Takayama, Ikoma, Nara 630-0192, Japan
[f] Present address: Center for Systems and Translational Brain Sciences, Institute of Human Complexity and Systems Science, System Science Center for Brain and Cognition, Yonsei University, 50 Yonsei-ro Seodaemun-gu, Seoul, 03722, Republic of Korea.
[g] Department of Chemistry and Biochemistry, Graduate School of Engineering, Kyushu University, 744 Moto-oka, Nishi-ku, Fukuoka 819-0395, Japan
[h] International Institute for Carbon Neutral Energy Research (WPI-I2CNER), Kyushu University, 744 Moto-oka, Nishi-ku, Fukuoka 819-0395, Japan
[i] Institute for Research Promotion and Collaboration, University of Hyogo, 123 Minamiekimae-cho, Himeji, Hyogo 670-0962, Japan
[j] Institute of Quantum Beam Science, Graduate School of Science and Engineering, Ibaraki University, 4-12-1 Nakanarusawa, Hitachi, Ibaraki 316-8511, Japan

[‡] These authors are contributed equally to this work.

[*] **Corresponding author**
Yoshiki Higuchi, Email: hig@sci.u-hyogo.ac.jp

Table of Contents

Mechanism of O_2-tolerance of the membrane-bound [NiFe]-hydrogenases. The cubane form of [4Fe-3S]$_P$ found in the H_2-reduced (HRED) state of the membrane-bound [NiFe]-hydrogenase (MBH-type) enzymes was deformed by the oxidation with $K_3[Fe(CN)_6]$ (FOXI), and Fe4 was coordinated by the deprotonated amide N^{1-4} and the glutamate (Glu76 for EcMBH and Glu82 for HmMBH) (Figs. S1A-S1C).[1,2] The EcMBH and additionally refined HmMBH in FOXI structures did not indicate a unique conformation of the glutamate (Figs. S1B, S1C and TableS1B).[1,2] Furthermore, the crystal structure of ReMBH in the air-oxidized state (AOXI) revealed an additional OH ligand at Fe1 (Fig. S1D),[3] which was detected in neither HmMBH nor EcMBH. According to electron paramagnetic resonance (EPR) studies and electrochemical measurements of MBH-type, [4Fe-3S]$_P$ has three oxidation states ([4Fe-3S]$_P^{3+/4+/5+}$).[5,6] In the catalytic cycle, the electrons produced by H_2 oxidation are sequentially supplied to the proximal, medial, and distal Fe-S clusters (Fig. S1F). When the enzymes are exposed to O_2, [4Fe-3S]$_P$ in MBH-type enzymes donates an additional electron back to the active site to reduce O_2 into H_2O, producing the super-oxidized state.[1,2,7] The negative charges of the deprotonated N and carboxylate near Fe4 in HmMBH and EcMBH, and OH at Fe1 in ReMBH[3] contribute to the stabilization of [4Fe-3S]$_P^{5+}$(Figs. S1B-S1D). Consequently, [4Fe-3S]$_P$ is considered to play an important role in O_2-tolerance of the enzymes in Group 1d.

SI Materials and Methods

Sample preparation and crystallization of [NiFe]-hydrogenase from *Citrobacter* sp. S-77. Bacterial cultivation and purification of the enzyme were performed similarly to a previously described protocol.[8,9] All chromatography procedures were carried out under anaerobic conditions. Protein samples for the crystallographic experiment under air-oxidized (AOXI) conditions and those for the spectroscopic measurements were prepared with trypsin treatment,[9] whereas crystals under H_2-reduced (HRED) and $K_3[Fe(CN)_6]$-oxidized (FOXI) conditions were prepared from the samples without trypsin treatment. Trypsin treatment of S77HYB prevented the protein from aggregating, especially for the AOXI samples, resulting in better recovery of the protein and diffraction of the crystals.[9] There was no explicit difference in the overall folding of the S77HYB under various redox conditions. Purified enzymes for both spectroscopic and crystallographic experiments were dialyzed against 10 mM MOPS-KOH (pH 7.0) and 200 mM NaCl prior to the experiments. The dialyzed protein solution was concentrated to 0.5 mM, 1 mM, and 15 mg mL^{-1} for EPR, FT-IR, and crystallization, respectively. Crystals were prepared by the sitting-drop vapor diffusion method at 283 K under aerobic conditions. To prepare the HRED crystals, AOXI crystals were soaked in a buffer containing 100 mM Tris-HCl (pH 8.5), 20% PEG10000, 200 mM NaCl, 20% glycerol, and 1 mM benzyl viologen in a screw capped vial with silicone septum, and the gas phase was replaced and incubated overnight at 283 K under H_2. To prepare the FOXI crystals, the HRED crystals were soaked in a buffer containing 100 mM Tris-HCl (pH 8.5), 20% PEG10000, 200 mM NaCl, 20% glycerol, and 5 mM $K_3[Fe(CN)_6]$ in a vial overnight at 283 K in a glove box. The protein droplet was prepared by mixing 0.5 µL of the protein solution consisting of 15 mg mL^{-1} S77HYB, 10 mM MOPS-KOH (pH 7.0), 200 mM NaCl and 0.5 µL of a reservoir solution including 100 mM Tris-HCl (pH 8.5), 19% PEG10000, 200 mM NaCl, and 20% glycerol, and was equilibrated against 70 µL of the reservoir solution. Brown crystals appeared within a few days. The AOXI crystals were frozen under aerobic conditions, whereas those in HRED and FOXI were frozen in the glovebox by liquid nitrogen. All crystals were stored in liquid nitrogen until use.

X-ray diffraction data collection and structure refinement. The X-ray diffraction datasets were collected using the BL44XU beamline of SPring-8 (Hyogo, Japan, proposal nos. 2014B6925 for HRED and 2015A6700 for FOXI and AOXI with the support of the staff at BL44XU and in part by the Platform for Drug Discovery, Informatics and Structural Life Science from MEXT.). Data processing, structure analysis, and refinement of S77HYB under various conditions were carried out. The crystals were

maintained at 100 K using a nitrogen gas stream during data collection. The diffraction data were integrated, scaled, and merged with the XDS program package.[10] The initial phase determination of the AOXI crystal structure was performed by the molecular replacement method using the program Phaser[11] of the CCP4 program suite[12] with atomic coordinates of the enzyme from *H. marinus* (PDB ID: 3AYZ) as the initial search model. Other structures were solved by molecular replacement using the AOXI S77HYB structure. Model building was performed using COOT.[13] Structure refinement in the early stage was carried out using Refmac5,[14] and Phenix[15] was used for subsequent refinement. Estimated radiation doses for the HRED, AOXI, and FOXI crystals calculated by RADDOSE-3D[16] were 0.67, 0.19, and 1.00 MGy, respectively. These doses were well below the Garman limit of 20 MGy.[17] The atomic parameters in multiple conformers ($[4Fe\text{-}4S]_P$ and Asp81) converged well with normal values in the crystallographic refinement, suggesting that there was no serious X-ray radiation damage to the structures. The positions of Fe in the deformed $[4Fe\text{-}4S]_P$ in FOXI were confirmed in the Bijvoet anomalous difference map (Fig. S2F, ESI). The multiple sequence alignment (*SI Appendix*, Fig. S6) was generated using Clustal Omega[18] and was shaped with ESPript 3.0[19] (http://espript.ibcp.fr).

EPR and FT-IR measurements. S77HYB (0.5–2.0 mM) (10 mM MOPS-KOH buffer (pH 7.0 at 274 K) containing 200 mM NaCl) and DvMSTD (25 mM Tris/HCl buffer (pH 8.0 at 274 K)) were transferred to 4 mm ϕ EPR tubes, degassed with a vacuum line, and purged with 1 bar of H_2. To obtain HRED samples, S77HYB and DvMSTD were incubated at 30 °C for 3 h and at 37 °C for 5.5 h, respectively. The HRED sample solution for the EPR measurements was degassed with a vacuum line and purged with 1 bar of N_2. The sample solution was further degassed with the vacuum line and purged with air to obtain AOXI samples. The FOXI sample was obtained by the anaerobic addition of 10 equivalents of $K_3[Fe(CN)_6]$ (Wako Pure Chemical Industries, Ltd., Osaka, Japan) under an N_2 atmosphere. The EPR spectra of [NiFe]-hydrogenase were measured at 77 K with an EPR spectrometer (JESFA100N; JEOL, Tokyo, Japan) and at 4–100 K with an EPR spectrometer (E-500; Bruker, Billerica, MA, USA). The spectra were averaged over five scans.

For FT-IR measurements, anaerobically isolated S77HYB (~1.2 mM) under a 97% N_2 and 3% H_2 atmosphere was transferred anaerobically to an infrared cell with CaF_2 windows in a glove box system (YSD-800L, UNICO, Tsukuba, Japan) prior to freezing in liquid N_2. FT-IR spectra of [NiFe]-hydrogenase were measured during light irradiation at 138–198 K with a FT-IR spectrometer (FT-IR 6100V; JASCO, Tokyo, Japan) equipped with an MCT detector. A cryostat system (CoolSpeK IR USP-203IR-A; Unisoku, Hirakata, Japan) was used to control the temperature of the cell. Spectral data were collected at a 2 cm^{-1} resolution and averaged over 1024 scans. The corresponding buffer spectrum was collected as a reference spectrum and subtracted from the sample spectra. The laser power for the light irradiation was adjusted to 0.5 W/cm^2 at the sample point.

A part of spectroscopic measurements was conducted in the Institute for Molecular Science, National Institute of Natural Sciences, supported by the Nanotechnology Platform Program (Molecule and Material Synthesis) of the Ministry of Education, Culture, Sports, Science and Technology of Japan (MEXT).

Computational Methods

***Ab initio* quantum mechanics (QM) calculations.** To explore the molecular species and the spin states of the crystallographically unassigned atoms (i.e., W2 and O1), *ab initio* electronic structure calculations of the distorted $[4Fe\text{-}4S]_P$ moiety found in the FOXI structure were performed. To perform *ab initio* electronic structure calculations, the deformed $[4Fe\text{-}4S]_P$ moiety in the super-oxidized state (FOXI crystal structure) was extracted from the atomic coordinates, which included four cysteine residues (i.e. Cys22, Cys25, Cys120, and Cys154), Asp81, W2, and a crystallographically unassigned atom

(tentatively assigned to O1 in Fig. 2B). Here, W2 and O1 are referred to as U_B and U_A in the theoretical calculation (*SI Appendix*, Table S2). The amino acid residues were truncated by replacing the C_α atoms with methyl groups, and the peptide bonds of Glu21-Cys22, Cys22-Thr23, Thr23-Gly24, Gly24-Cys25, Asp81-Gly82, Ile117-Gly118, and Cys120-Ala121 were included in the structural models. To identify the species of the unassigned atoms together with the precise positions, H_2O, HO^-, O^{2-}, O^-, HS^-, or S^{2-} were assigned to U_A, and H_2O or HO^- was assigned to U_B in the models. Thus, 12 structural models were examined by employing the geometry optimization (*SI Appendix*, Table S2).

For $[4Fe\text{-}4S]_P$ in the crystal structure, each of the Fe ions forms the tetrahedral structure with the coordinated atoms, and the charge and spin states of each Fe ion would be Fe^{2+} or Fe^{3+}, and 4/2 or 5/2, respectively.[20,21] The super-oxidized state would further restrict the possible combinations of Fe^{2+} and Fe^{3+}. Here, we can also refer to the optimum charge and spin states that were elucidated in previous studies of the proximal clusters of MBH-type enzymes,[5,22] which also exhibit oxygen tolerance. Thereby, we assume that the appropriate charge and spin states of the [4Fe-4S] core in the super-oxidized state are +3 and 1/2, respectively, and thus infer that the [4Fe-4S] core consists of 1 Fe^{2+} and 3 Fe^{3+}. The total charge and spin states of the present models are shown in *SI Appendix*, Table S2.

Owing to the tetrahedral structure of the Fe ions in $[4Fe\text{-}4S]_P$, all Fe ions are assumed to exhibit high spin states,[20,21] and thus the combinations of the spin states of the four Fe ions are restricted; that is, two Fe ions are +5/2 and the others are -4/2 and -5/2. This condition is imposed to determine the spin states, as follows. To assign the spin states of the [4Fe-4S] core, the nomenclature BSij is used. BS is an acronym for the broken symmetry state,[23] and i and j indicate the numbers of Fe ions where -4/2 and -5/2 are assigned, respectively.[20,21] For example, BS12 indicates that the spin states of Fe1 and Fe2 are -4/2 and -5/2, respectively (accordingly, those of Fe3 and Fe4 are both +5/2). The spin assignments of the Fe ions are described as (Fe1, Fe2, Fe3, Fe4) = (-4/2, -5/2, +5/2, +5/2), and thus the total spin is 1/2. For quantum mechanical calculations, six spin assignments (BS12, BS13, BS14, BS23, BS24, and BS34) were imposed with respect to each of the 12 models (*SI Appendix*, Table S2).

All *ab initio* calculations were performed employing Gaussian09,[24] and all-electron hybrid spin-unrestricted Hartree–Fock/density functional theory calculations used the B3LYP functional.[25,26] The triple-ζ valence polarized basis set[27] was applied to the Fe ions, the atoms that directly coordinate to the Fe ions, and the species relevant to U_A and U_B. For the remaining atoms, the 6-311G** basis set was adopted. As mentioned, for each of 12 models, six spin states were examined in the following calculations (in total, 72 calculations were performed), as mentioned above. For geometry optimization, the following three-step procedure was adopted. First, only hydrogen atoms were movable. Second, only the molecular species including U_A and U_B atoms were movable, and then Fe and S ions were also movable together with the U_A and U_B species, where the other atoms in the models were fixed.

MD calculations. MD simulations of the fully solvated modeled structures were performed to theoretically investigate the distributions of the water molecules theoretically in each of the proximal clusters of S77HYB and standard hydrogenase (DvMSTD). The crystal structure for *Ralstonia eutropha* (ReMBH) (PDB ID: 4IUD) was employed as the initial structure for modeling of the fully solvated systems of S77HYB and standard hydrogenase (DvMSTD) (hereafter, the initial system is also termed the reference structure), and the hydrogen atoms were attached by employing the LEAP module in the amber12 program package.[28] Then, box water with a solvent distance of 12 Å from the enzyme was set. The force field parm99SB was adopted to evaluate the energy function, and all MD calculations were performed using the sander module in the amber12 suite. To relax the configuration of solvent water molecules, energy minimizations and MD simulations were performed by employing the following three-step procedure. First, the configurations of the hydrogen atoms of the box water were optimized by performing i) 1,000-step energy minimization, ii) 10 ps MD simulation at 300 K, and finally iii) 1,000-

step energy minimization. Second, this type of three-step procedure was adopted to optimize the configurations of the hydrogen atoms of the box water together with those of the crystal water. Finally, all hydrogen atoms in the system were optimized by 1,000-step energy minimization. In all of these relaxation procedures, the other moieties (e.g. the heavy atoms of the enzyme) were restrained by a harmonic potential with a 100 kcal/mol·Å^2 force constant. Then, to relax the configuration of the solvent water molecules, a 10 ps MD simulation was performed, where a harmonic constraint was applied to all heavy atoms of the enzyme with a force constant of 100 kcal/mol·Å^2. The force constant was then reduced to 50, 25, 10, 5, 4, and 1 kcal/mol·Å^2 in six MD simulations, and the time of each simulation was 5 ps. Employing the resultant system, the fully solvated S77HYB and DvMSTD structures were built by replacing the atomic coordinates of the corresponding regions. A water molecule postulated to be generated in the reduction of the proximal cluster was added to a site close to Fe2. The structures were carefully relaxed by multistep combined energy minimization and MD simulations. Then, for each of the fully solvated S77HYB and DvMSTD structures, the 5 ns MD simulations were conducted for structural relaxation. Then, for each of the distinct 32 replicas of each system, 5 ns productive MD simulations were performed using different sets of initial velocities to generate a structural ensemble. In total, 160 ns MD simulations were performed for each system.

Computational Analysis Results

Identification of crystallographically unassigned species by *ab initio* QM calculations. To identify the crystallographically unassigned species (represented by U_A and U_B), the most stable spin state was explored by adopting six possible spin states in each of the 12 structural models (for each of the 72 conditions, geometry optimization was conducted). Then, the obtained structures were compared with the crystal structure. With respect to the U_A and U_B species, Model 2 in the BS34 spin state exhibited the smallest deviations (0.12 Å) among all the models (*SI Appendix*, Table S2 and Fig. S4), and was also smallest in terms of the root-mean-square deviation of $[4Fe\text{-}4S]_P$ and the heavy atoms of the U_A and U_B species in the comparison with the crystal structure (0.198 Å).

For Model 7 in the BS34 spin state, geometry optimization was started from the distinct initial configuration of the U_A and U_B species, and the obtained configuration and geometry were almost identical to those of Model 2. In particular, the U_A species (H_2O) was dissociated into OH^- and H^+, the latter of which attached to the U_B species, thereby forming an H_2O. Additionally, note that Model 7 in the BS34 spin state exhibited the second smallest deviations for U_A and U_B (i.e. 0.12 and 0.15 Å, respectively) (*SI Appendix*, Table S2) in terms of the crystal structure. Thus, Models 2 and 7 in the BS34 spin state were consistent with the geometry of the crystal structure, whereas the other models were not. In summary, we concluded that U_A and U_B were an OH^- and H_2O.

Evaluation of the mobility of water molecules around $[4Fe\text{-}4S]_P$ of S77HYB and DvMSTD by MD simulations. In standard hydrogenases with $[4Fe\text{-}4S]_P$, His13-Ala14/Asn14-Ala15-Glu16 residues are well conserved (this numbering system is based on that of DvMSTD), and thus His13 apparently blocks the channel that is connected from the core moiety of the proximal cluster to the outside of the enzyme. In contrast, His13 of standard hydrogenases is replaced with Gly18 in S77HYB, which leads the channel to extension from the inside close to the proximal cluster to the outside of the enzyme. This difference in the amino acid residues (His13 vs Gly18) may influence the mobility of the water molecules located around the proximal clusters (Figs. 3C and 3D). We evaluated the effects of differences in such amino acid residues on the mobility of water molecules in the proximal cluster by the MD simulations.

This analysis indicated that in the DvMSTD structure, the water molecule that was postulated to be generated in the reduction of the proximal cluster was stably located close to Fe2 (Fig. 3C), whereas in S77HYB, the corresponding water was dislocated toward Gly18, thereby forming a hydrogen bond with one of the water molecules included in a water array near Gly18 (Fig. 3D). The generated water or water

proton could be expelled towards the outside of the S77HYB structure, because the water array was connected to the bulk water.

References:

1. Y. Shomura, K.-S. Yoon, H. Nishihara and Y. Higuchi, *Nature*, 2011, **479**, 253–257.
2. A. Volbeda, P. Amara, C. Darnault, J.-M. Mouesca, A. Parkin, M. M. Roessler, F. A. Armstrong and J. C. Fontecilla-Camps, *Proc. Natl. Acad. Sci. U. S. A.*, 2012, **109**, 5305–5310.
3. S. Frielingsdorf, J. Fritsch, A. Schmidt, M. Hammer, J. Löwenstein, E. Siebert, V. Pelmenschikov, T. Jaenicke, J. Kalms, Y. Rippers, F. Lendzian, I. Zebger, C. Teutloff, M. Kaupp, R. Bittl, P. Hildebrandt, B. Friedrich, O. Lenz and P. Scheerer, *Nat. Chem. Biol.*, 2014, **10**, 378–385.
4. J. Fritsch, P. Scheerer, S. Frielingsdorf, S. Kroschinsky, B. Friedrich, O. Lenz and C. M. T. Spahn, *Nature*, 2011, **479**, 249–252.
5. M.-E. Pandelia, D. Bykov, R. Izsak, P. Infossi, M.-T. Giudici-Orticoni, E. Bill, F. Neese and W. Lubitz, *Proc. Natl. Acad. Sci. USA*, 2013, **110**, 483–488.
6. M. M. Roessler, R. M. Evans, R. A. Davies, J. Harmer and F. A. Armstrong, *J. Am. Chem. Soc.*, 2012, **134**, 15581–15594.
7. T. Goris, A. F. Wait, M. Saggu, J. Fritsch, N. Heidary, M. Stein, I. Zebger, F. Lendzian, F. A. Armstrong, B. Friedrich and O. Lenz, *Nat. Chem. Biol.*, 2011, **7**, 310–318.
8. S. Eguchi, K. S. Yoon and S. Ogo, *J. Biosci. Bioeng.*, 2012, **114**, 479–484.
9. N. D. Muhd Noor, K. Nishikawa, H. Nishihara, K.-S. Yoon, S. Ogo and Y. Higuchi, *Acta Crystallogr. F Struct. Biol. Commun.*, 2016, **72**, 53–58.
10. W. Kabsch, *Acta Crystallogr. Sect. D Biol. Crystallogr.*, 2010, **66**, 125–132.
11. A. J. McCoy, R. W. Grosse-Kunstleve, P. D. Adams, M. D. Winn, L. C. Storoni and R. J. Read, *J. Appl. Crystallogr.*, 2007, **40**, 658–674.
12. M. D. Winn, C. C. Ballard, K. D. Cowtan, E. J. Dodson, P. Emsley, P. R. Evans, R. M. Keegan, E. B. Krissinel, A. G. W. Leslie, A. McCoy, S. J. McNicholas, G. N. Murshudov, N. S. Pannu, E. A. Potterton, H. R. Powell, R. J. Read, A. Vagin and K. S. Wilson, *Acta Crystallogr. Sect. D Biol. Crystallogr.*, 2011, **67**, 235–242.
13. P. Emsley, B. Lohkamp, W. G. Scott and K. Cowtan, *Acta Crystallogr. Sect. D Biol. Crystallogr.*, 2010, **66**, 486–501.
14. G. N. Murshudov, P. Skubák, A. A. Lebedev, N. S. Pannu, R. A. Steiner, R. A. Nicholls, M. D. Winn, F. Long and A. A. Vagin, *Acta Crystallogr. Sect. D Biol. Crystallogr.*, 2011, **67**, 355-367.
15. P. D. Adams, P. V. Afonine, G. Bunkóczi, V. B. Chen, I. W. Davis, N. Echols, J. J. Headd, L. W. Hung, G. J. Kapral, R. W. Grosse-Kunstleve, A. J. McCoy, N. W. Moriarty, R. Oeffner, R. J. Read, D. C. Richardson, J. S. Richardson, T. C. Terwilliger and P. H. Zwart, *Acta Crystallogr. Sect. D Biol. Crystallogr.*, 2010, **66**, 213–221.
16. O. B. Zeldin, M. Gerstel and E. F. Garman, *J. Appl. Crystallogr.*, 2013, **46**, 1225–1230.
17. R. L. Owen, E. Rudino-Pinera and E. F. Garman, *Proc. Natl. Acad. Sci. U. S. A.*, 2006, **103**, 4912–4917.
18. M. A. Larkin, G. Blackshields, N. P. Brown, R. Chenna, P. A. Mcgettigan, H. McWilliam, F. Valentin, I. M. Wallace, A. Wilm, R. Lopez, J. D. Thompson, T. J. Gibson and D. G. Higgins, *Bioinformatics*, 2007, **23**, 2947-2948.
19. P. Gouet, X. Robert and E. Courcelle, *Nucleic Acids Res.*, 2003, **31**, 3320-3323.
20. V. Pelmenschikov and M. Kaupp, *J. Am. Chem. Soc.*, 2013, **135**. 11809-11823.
21. S. G. Tabrizi, V. Pelmenschikov, L. Noodleman and M. Kaupp, *J. Chem. Theory Comput.*, 2016, **12**, 174-187.

22. M. E. Pandelia, W. Nitschke, P. Infossi, M.-T. Giudici-Orticoni, E. Bill and W. Lubitz, *Proc. Natl. Acad. Sci. U. S. A.*, 2011, **108**, 6097–6102.
23. L. Noodleman and D. A. Case, *Adv. Inorg. Chem.*, 1992, **38**, 423-470.
24. G. M. J. Frisch, W. Trucks, H. B. Schlegel, G. E. Scuseria, M. A. Robb, J. R. Cheeseman, G. Scalmani, V. Barone, B. Mennucci, G. A. Petersson, H. Nakatsuji, M. Caricato, X. Li, H. P. Hratchian, A. F. Izmaylov, J. Bloino, G. Zheng and J. L. Sonnenberg, *Inc. Wallingford, CT*, 2009.
25. C. Lee, W. Yang and R. G. Parr, *Phys. Rev. B*, 1988, **37**, 785-789.
26. A. D. Becke, *Phys. Rev. A*, 1993, **98**, 5648-5652.
27. A. Schäfer, H. Horn and R. Ahlrichs, *J. Chem. Phys.*, 1992, **97**, 2571-2577.
28. D. A. Case, T.A. Darden, T.E. Cheatham, III, C.L. Simmerling, J. Wang, R.E. Duke, R. Luo, R.C. Walker, W. Zhang, K.M. Merz, B. Roberts, S. Hayik, A. Roitberg, G. Seabra, J. Swails, A.W. Götz, I. Kolossváry, K.F. Wong, F. Paesani, J. Vanicek, R.M. Wolf, J. Liu, X. Wu, S.R. Brozell, T. Steinbrecher, H. Gohlke, Q. Cai, X. Ye, J. Wang, M.-J. Hsieh, G. Cui, D.R. Roe, D.H. Mathews, M.G. Seetin, R. Salomon-Ferrer, C. Sagui, V. Babin, T. Luchko, S. Gusarov, A. Kovalenko, and P.A. Kollman , 2012, University of California, San Francisco.

SI Figures

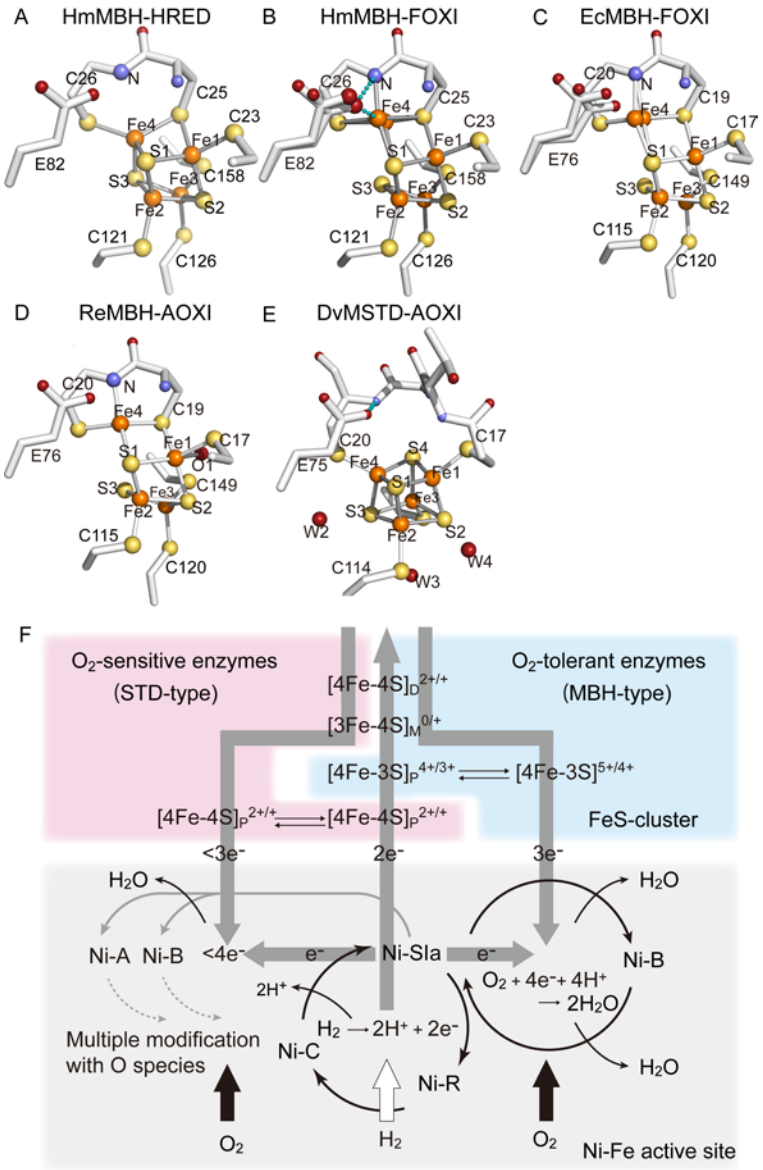

Fig. S1.

Structures of $[4Fe\text{-}3S]_P$ of MBH-type O_2-tolerant [NiFe]-hydrogenases in various redox conditions with that of $[4Fe\text{-}4S]_P$ of O_2-sensitive AOXI DvMSTD and the O_2-tolerant mechanism. In $[4Fe\text{-}3S]_P$, one of four sulfides (S4) in a $[4Fe\text{-}4S]_P$ type cluster is replaced by nearby cysteine thiolate and another cysteine takes part in the coordination to iron atoms. The structures of $[4Fe\text{-}3S]_P$ of HRED HmMBH (A), FOXI HmMBH (B), FOXI EcMBH (C), AOXI ReMBH (D), and AOXI DvMSTD (E) (atom colors: C, gray; N, blue; O, red; S, yellow; Fe, orange). (F) O_2-tolerant molecular mechanism based on the experimental data obtained from MBH-type enzymes with that from O_2-sensitive STD-type enzymes. The vertical thick gray arrows indicate the electron flow from (to) the active site to (from) the Fe-S clusters. The upward arrow shows the electron flow of the H_2-uptake reaction from the active site to the clusters in the reduced state, whereas the downward one shows the back flow of the electrons when the enzyme is oxidized. The horizontal one indicates the electron donation from Ni-SIa. The pink and blue backgrounds indicate the electron flow through three Fe-S clusters in the O_2-sensitive and O_2-tolerant enzymes, respectively.

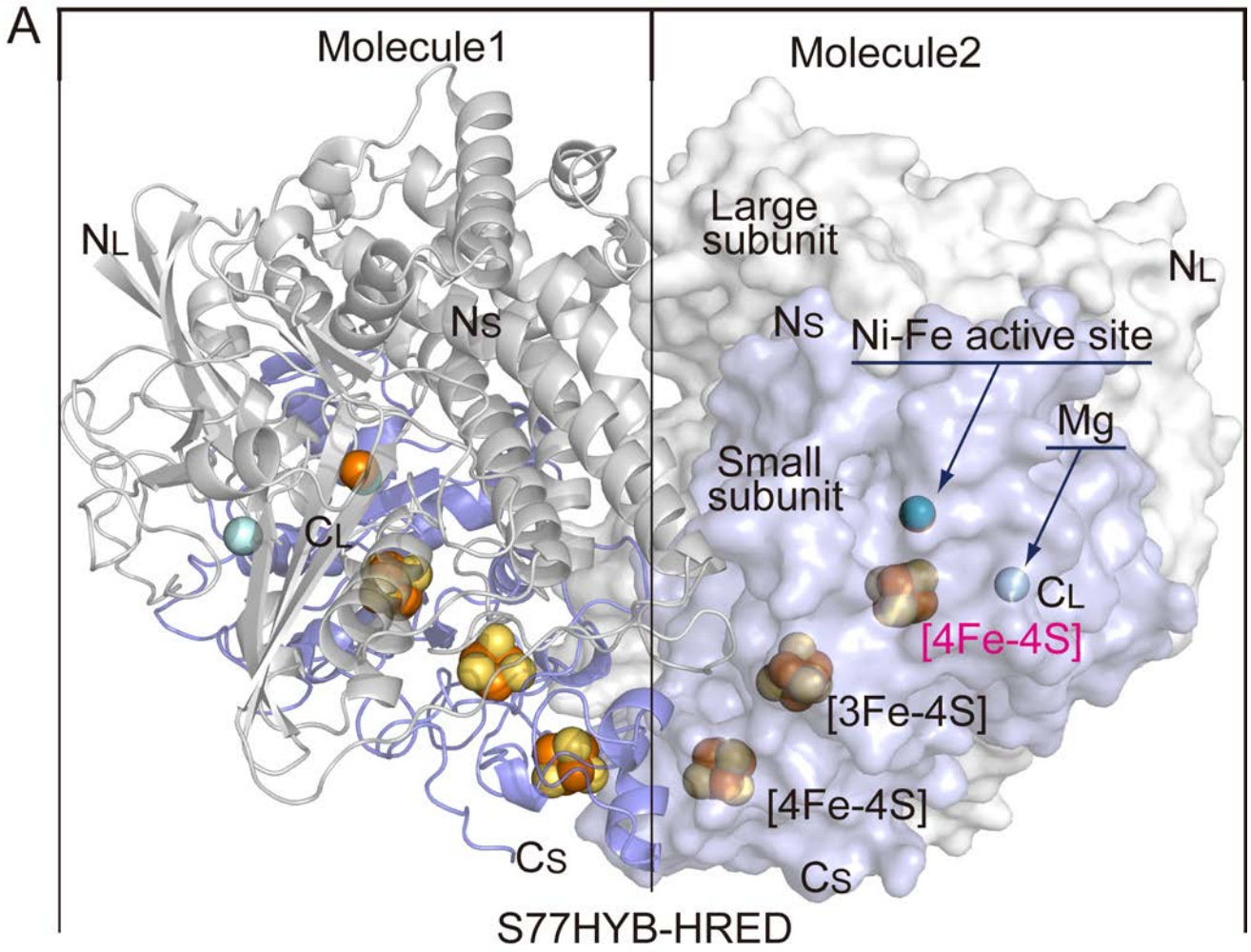
A
Molecule1
Molecule2
NL
Ns
CL
Cs
Large subunit
NL
Ns
Ni-Fe active site
Mg
Small subunit
CL
[4Fe-4S]
[3Fe-4S]
[4Fe-4S]
Cs
S77HYB-HRED

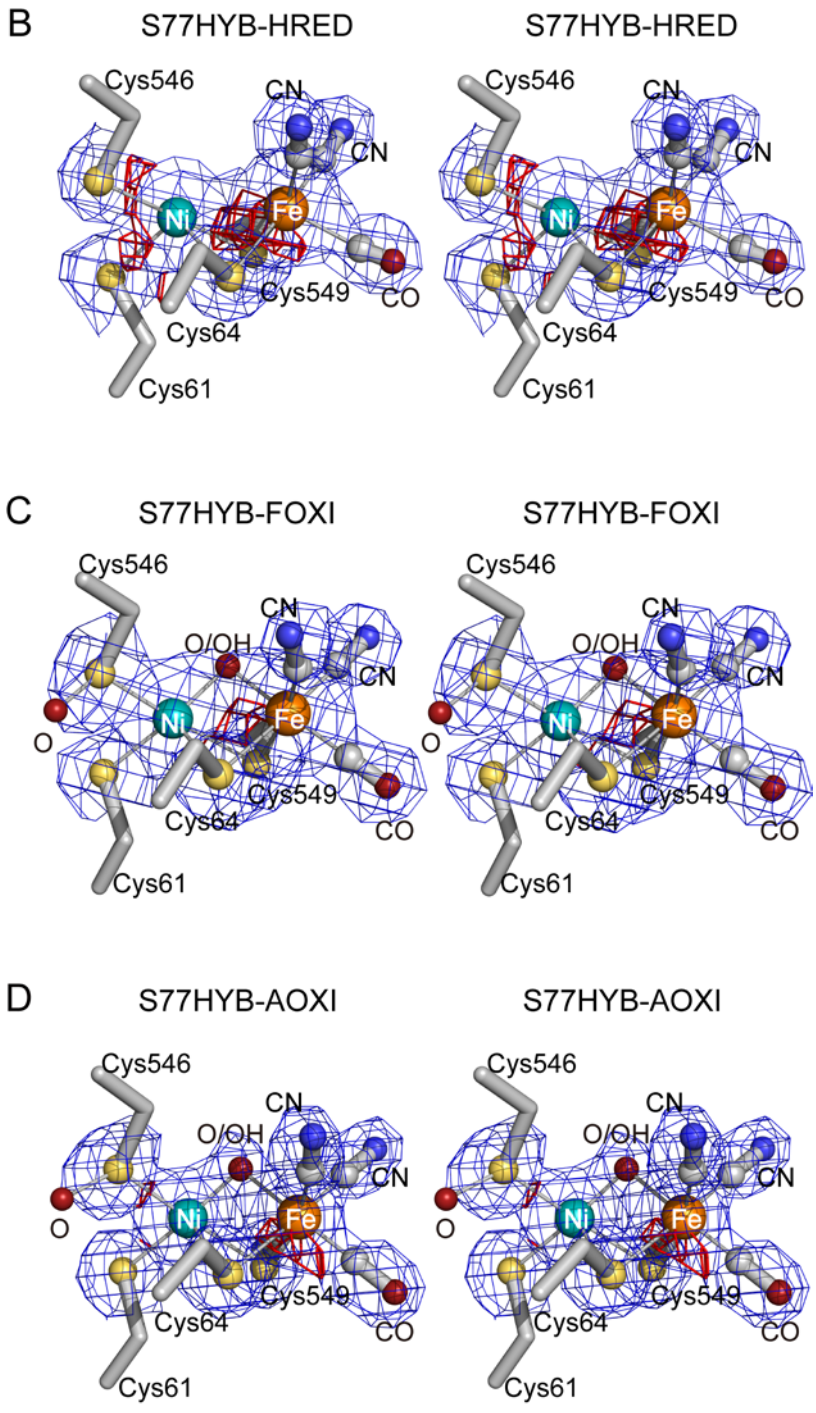
B
S77HYB-HRED
S77HYB-HRED
Cys546
CN
CN
Ni
Fe
Cys549
CO
Cys64
Cys61
C
S77HYB-FOXI
S77HYB-FOXI
O/OH
O
D
S77HYB-AOXI
S77HYB-AOXI

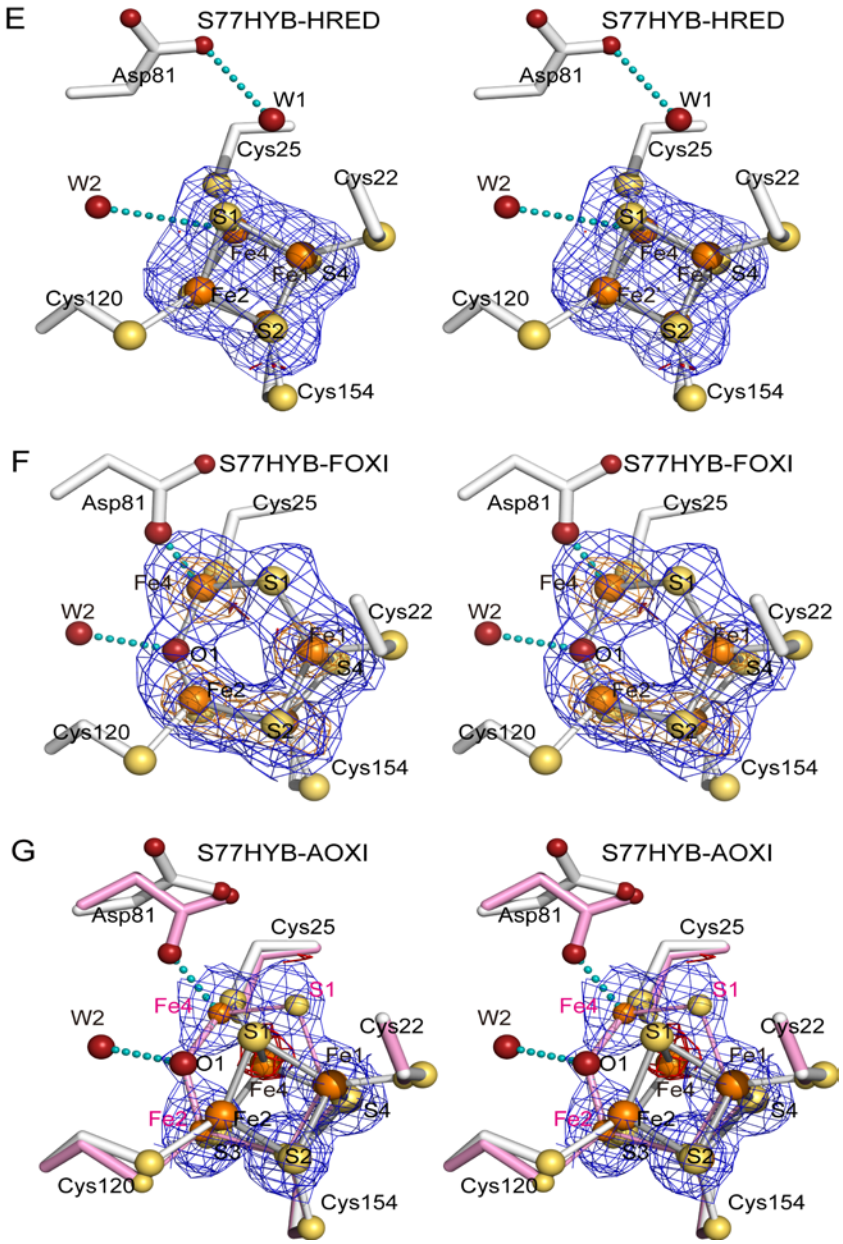

Fig. S2.

Crystal structure of [NiFe]-hydrogenase from *Citrobacter* sp. S-77 (S77HYB) in the HRED state and the Ni-Fe active site in the various states. Overall structure of the dimer of heterodimer of S77HYB (A) and stereo views of the model around the Ni-Fe active site of (B) HRED, (C) FOXI, and (D) AOXI S77HYB crystals, and those around $[4Fe\text{-}4S]_P$ of (E) HRED, (F) FOXI, and (G) AOXI S77HYB crystals with electron density maps. 2*F*o-*F*c (blue) and *F*o-*F*c (red) electron density maps for (B-F) are contoured at 1.5 σ and 3 σ, respectively. For FOXI $[4Fe\text{-}4S]_P$ (F), the anomalous difference map (yellow, λ=0.90000 Å of x-ray) is contoured at 3 σ in order to confirm the positions of Fe. For AOXI $[4Fe\text{-}4S]_P$ (G), the normal (red) and omitted (blue) difference Fourier maps are calculated and contoured at 3 σ. For the omitted difference map, the Fe and S atoms in the deformed components (occupancy = 0.5) in the cubane conformation are omitted for calculating *F*c. The atomic bonds in the conformer that appeared upon oxidation are depicted in pink in (G) (atom colors: C, gray; N, blue; O, red; S, yellow; Fe, orange; Ni, green).

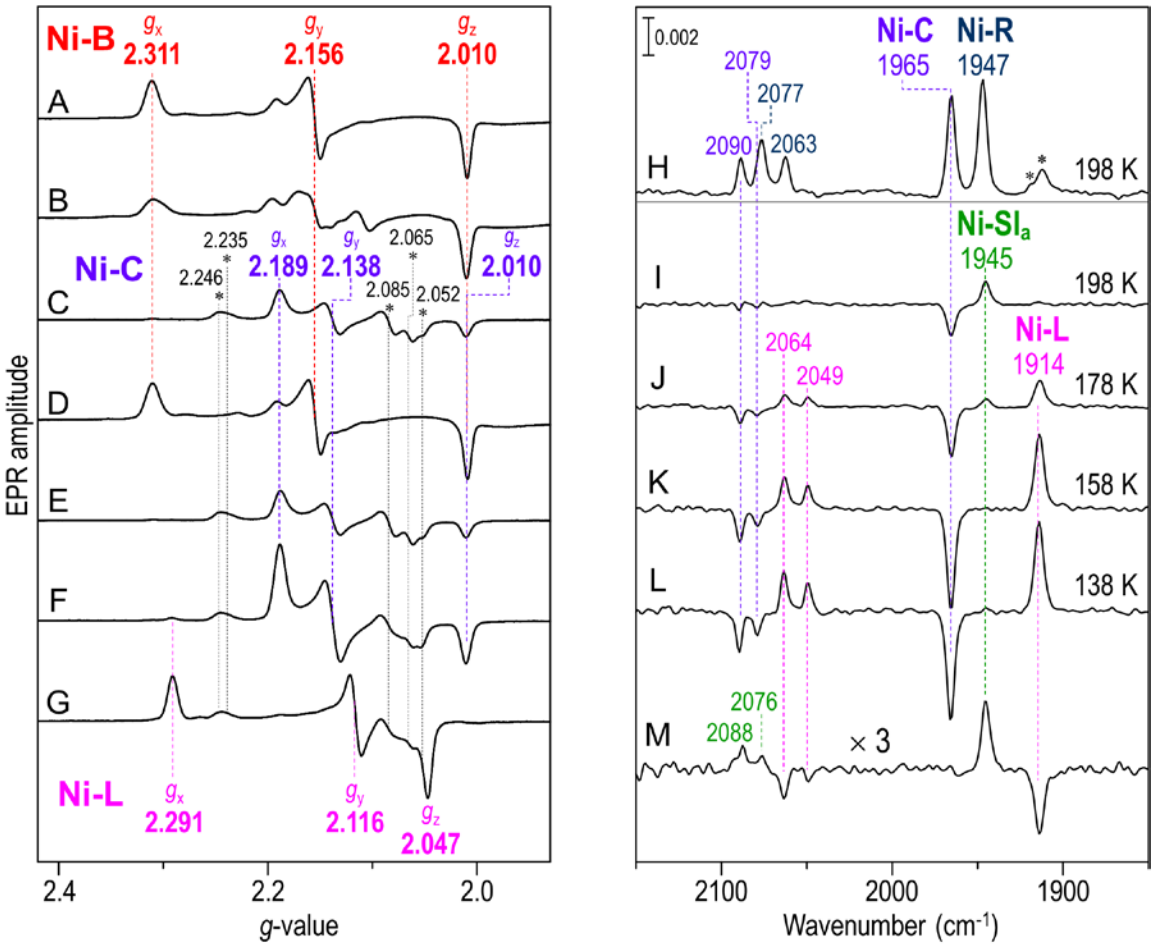

Fig. S3.

EPR and FT-IR spectra of [NiFe]-hydrogenase from *Citrobacter* sp. S-77: (A-G) EPR and (H–M) FT-IR spectra. (A) AOXI enzyme under an N_2 atmosphere, (B) FOXI enzyme under an N_2 atmosphere, (C) HRED enzyme under an H_2 atmosphere, (D) re-AOXI enzyme under an N_2 atmosphere, (E) re-HRED enzyme under an H_2 atmosphere, (F) re-HRED enzyme under an N_2 atmosphere, (G) light-irradiated re-HRED enzyme under an N_2 atmosphere (spectra recording was started after 45 min of irradiation), (H) before light irradiation, (I–L) difference between spectra during and before irradiation, and (M) calculated spectrum; (spectrum I) − 0.32 × (spectrum L). Spectrum M is magnified by ×3. Asterisks represent unidentified signals. Measurement conditions: (A–G) microwave frequency, 9.044 GHz; microwave power, 2 mW; modulation amplitude, 10 G; pH 7.0; 77 K; (H–L) under a 97% N_2 and 3% H_2 atmosphere; pH 7.0; (H and I) 198 K, (J) 178 K, (K) 158 K, and (L) 138 K.

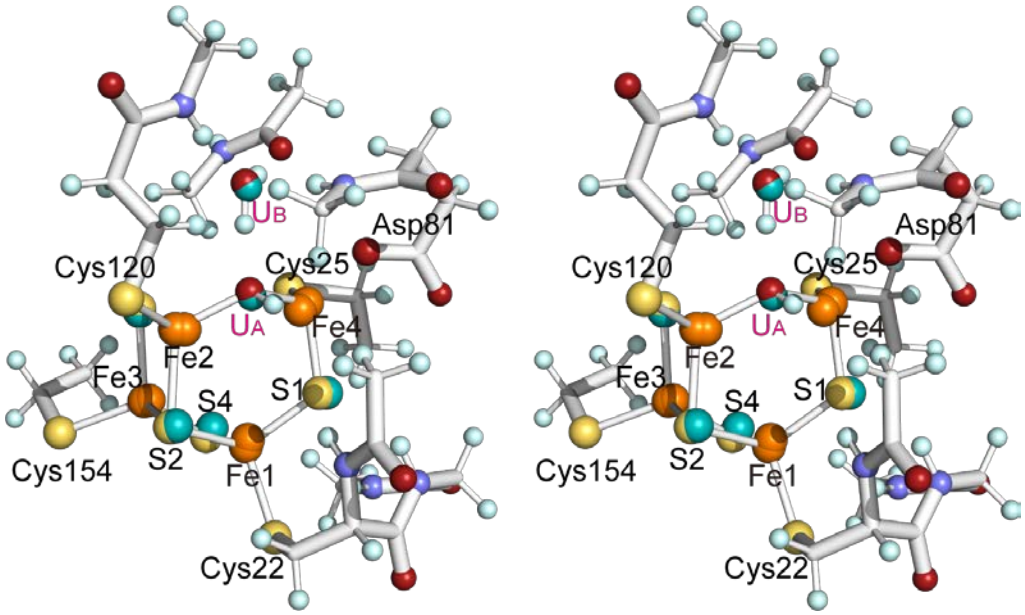

Fig. S4.

Stereo view of the most energetically favorable structure obtained by the geometry optimization of Model 2 (atom colors: C, white; N, blue; O, red; H, light cyan; S, yellow; Fe, orange), and the crystal structure of the proximal cluster (light green). For the moiety composed of the [4Fe-4S] core, U_A, and U_B, the RMSD is 0.198 Å with respect to the crystal structure, and for U_A and U_B atoms solely, it is 0.054 Å. Thus, U_A and U_B were identified as OH^- and a water molecule by theoretical calculations.

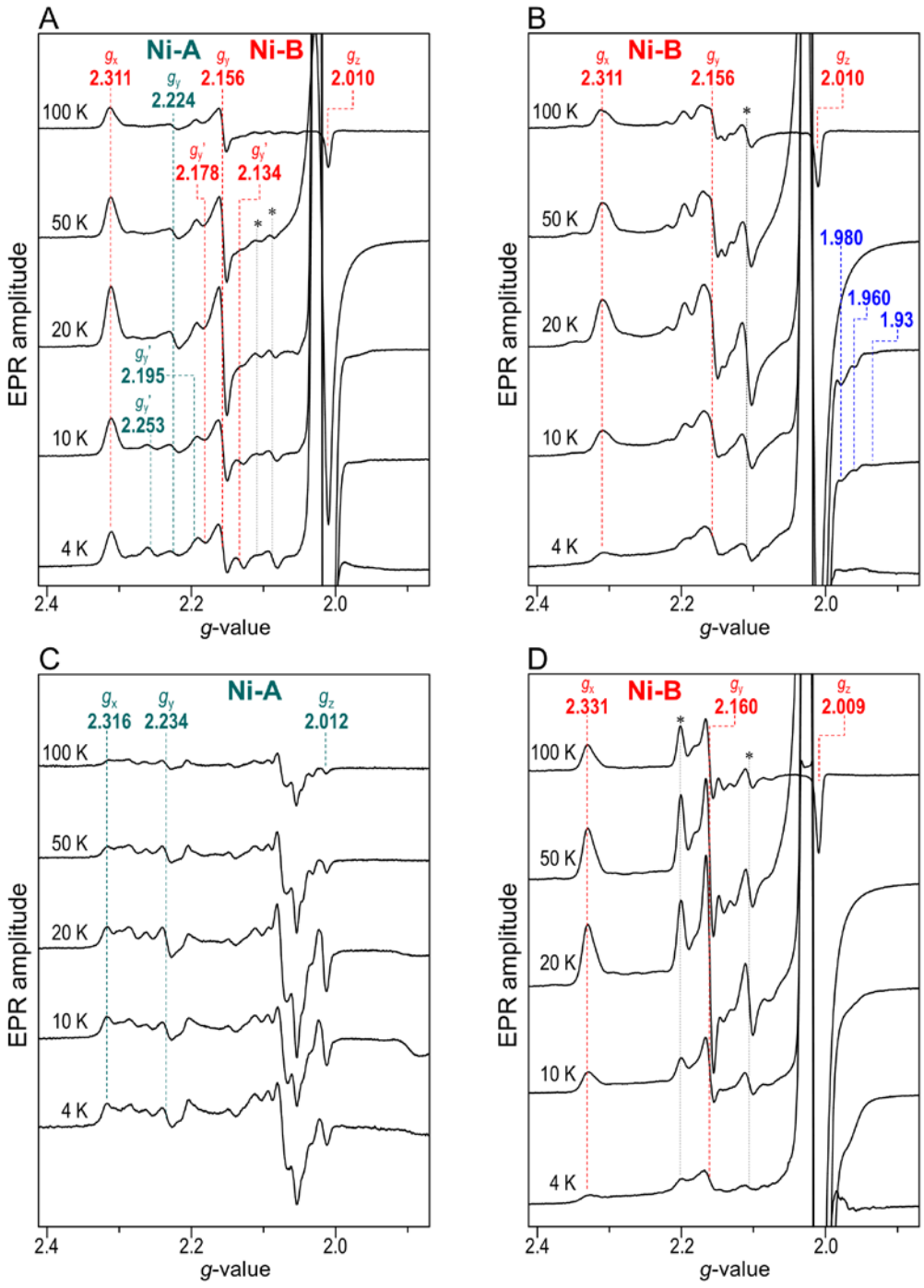

Fig. S5.

EPR spectra of [NiFe]-hydrogenase from (A, B) S77HYB and (C, D) DvMSTD. (A, C) AOXI and (B, D) FOXI enzymes. Asterisks represent unassigned signals. Measurement conditions: microwave frequency, 9.672 GHz; microwave power, 2 mW; modulation amplitude, 10 G; N_2 atmosphere; pH 7.0; 4–100 K. For S77HYB, the AOXI spectra exhibited the splitting of the Ni-signals, whereas the FOXI spectra exhibited new signals at g = 1.93, 1.96, and 1.98.

A

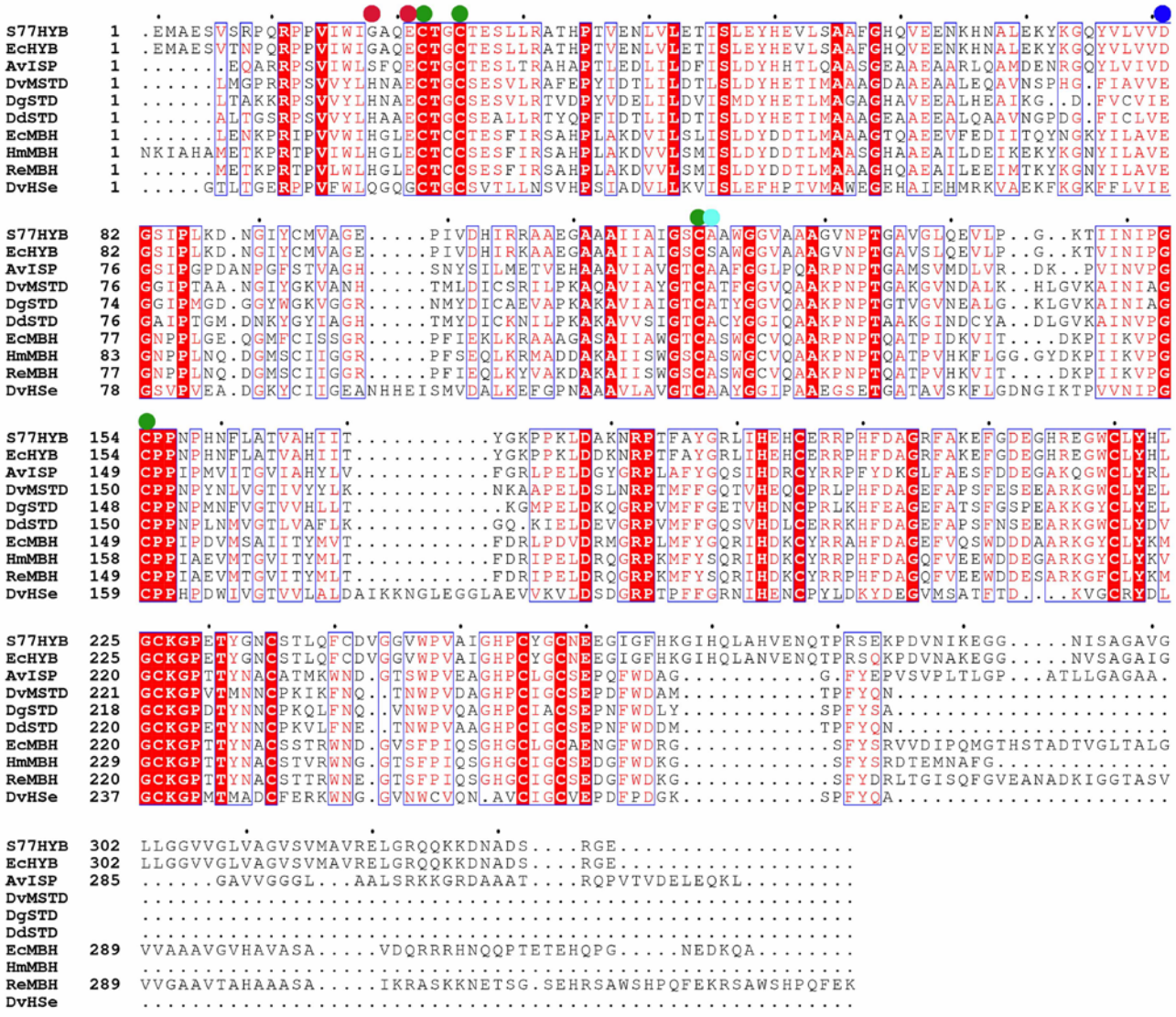
S77HYB 1 .EMAESVSRPQRPPVIWIGAQECTGCTESLLRATHPTVENLVLETISLEYHEVLSAAFGHQVEENKHNALEKYKGQQYVLVVD
EcHYB 1 .EMAESVTNPQRPPVIWIGAQECTGCTESLLRATHPTVENLVLETISLEYHEVLSAAFGHQVEENKHNALEKYKGQQYVLVVD
AvISP 1 .......EQARRPSVIWLSFQECTGCTESLTRAHAPTLEDLILDFISLDYHHTLQAASGEAAEAARLQAMDENRGQQYLVIVD
DvMSTD 1 ......LMGPRRPSVVYLHNAECTGCSESVLRAFEPYIDTLILDTLSLDYHETIMAAAGDAAEAALEQAVNSPHG.FIAVVE
DgSTD 1 ......LTAKKRPSVVYLHNAECTGCSESVLRTVDPYVDELILDVISMDYHETLMAGAGHAVEEALHEAIKG..D.FVCVIE
DdSTD 1 ......ALTGSRPSVVYLHAAECTGCSEALLRTYQPFIDTLILDTISLDYHETIMAAAGEAAEEALQAAVNGPDG.FICLVE
EcMBH 1 ......LENKPRIPVVWIHGLECTCCTESFIRSAHPLAKDVILSLISLDYDDTLMAAAGTQAEEVFEDIITQYNGKYILAVE
HmMBH 1 NKIAHAMETKPRTPVIWLHGLECTCCSESFIRSAHPLAKDVVLSMISLDYDDTLMAASGHAAEAILDEIKEKYKGNYILAVE
ReMBH 1 ......METKPRTPVLWLHGLECTCCSESFIRSAHPLAKDVVLSMISLDYDDTLMAAAGHQAEAILEEIMTKYKGNYILAVE
DvHSe 1 .....GTLTGERPPVFWLQGQGCTGCSVTLLNSVHPSIADVLLKVISLEFHPTVMAWEGEHAIEHMRKVAEKFKGKFFLVIE
S77HYB 82 GSIPLKD.NGIYCMVAGE.....PIVDHIRRAAEGAAAIIAIGSCAAWGGVAAAGVNPTGAVGLQEVLP..G..KTIINIPG
EcHYB 82 GSIPLKD.NGIYCMVAGE.....PIVDHIRKAAEGAAAIIAIGSCSAWGGVAAAGVNPTGAVSLQEVLP..G..KTVINIPG
AvISP 76 GSIPGPDANPGFSTVAGH.....SNYSILMETVEHAAAVIAVGTCAAFGGLPQAARPNPTGAMSVMDLVR..DK..PVINVPG
DvMSTD 76 GGIPTAA.NGIYGKVANH.....TMLDICSRILPKAQAVIAYGTCATFGGVQAAKPNPTGAKGVNDALK..HLGVKAINIAG
DgSTD 74 GGIPMGD.GGYWGKVGGR.....NMYDICAEVAPKAKAVIAIGTCATYGGVQAAKPNPTGTVGVNEALG..KLGVKAINIAG
DdSTD 76 GAIPTGM.DNKYGYIAGH.....TMYDICKNILPKAKAVVSIGTCACYGGIQAAKPNPTAAKGINDCYA..DLGVKAINVPG
EcMBH 77 GNPPLGE.QGMFCISSGR.....PFIEKLKRAAAGASAIIAWGTCASWGCVQAARPNPTQATPIDKVIT....DKPIIKVPG
HmMBH 83 GNPPLNQ.DGMSCIIGGR.....PFSEQLKRMADDAKAIISWGSCASWGCVQAAKPNPTQATPVHKFLGG.GYDKPIIKVPG
ReMBH 77 GNPPLNQ.DGMSCIIGGR.....PFIEQLKYVAKDAKAIISWGSCASWGCVQAAKPNPTQATPVHKVIT....DKPIIKVPG
DvHSe 78 GSVPVEA.DGKYCIIGEANHHEISMVDALKEFGPNAAAVLAVGTCAAYGGIPAAEGSETGATAVSKFLGDNGIKTPVVNIPG
S77HYB 154 CPPNPHNFLATVAHIIT..........YGKPPKLDAKNRPTFAYGRLIHEHCERRPHFDAGRFAKEFGDEGHREGWCLYHL
EcHYB 154 CPPNPHNFLATVAHIIT..........YGKPPKLDDKNRPTFAYGRLIHEHCERRPHFDAGRFAKEFGDEGHREGWCLYHL
AvISP 149 CPPIPMVITGVIAHYLV..........FGRLPELDGYGRPLAFYGQSIHDRCYRRPFYDKGLFAESFDDEGAKQGWCLYRL
DvMSTD 150 CPPNPYNLVGTIVYYLK..........NKAAPELDSLNRPTMFFGQTVHEQCPRLPHFDAGEFAPSFESEEARKGWCLYEL
DgSTD 148 CPPNPMNFVGTVVHLLT..........KGMPELDKQGRPVMFFGETVHDNCPRLKHFEAGEFATSFGSPEAKKGYCLYEL
DdSTD 150 CPPNPLNMVGTLVAFLK..........GQ.KIELDEVGRPVMFFGQSVHDLCERRKHFDAGEFAPSFNSEEARKGWCLYDV
EcMBH 149 CPPIPDVMSAIITYMVT..........FDRLPDVDRMGRPLMFYGQRIHDKCYRRAHFDAGEFVQSWDDDAARKGYCLYKM
HmMBH 158 CPPIAEVMTGVITYMLT..........FDRIPELDRQGRPKMFYSQRIHDKCYRRPHFDAGQFVEEWDDEGARKGYCLYKV
ReMBH 149 CPPIAEVMTGVITYMLT..........FDRIPELDRQGRPKMFYSQRIHDKCYRRPHFDAGQFVEEWDDESARKGFCLYKM
DvHSe 159 CPPHPDWIVGTVVLALDAIKKNGLEGGLAEVVKVLDSDGRPTPFFGRNIHENCPYLDKYDEGVMSATFTD..KVGCRYDL
S77HYB 225 GCKGPETYGNCSTLQFCDVGGVWPVAIGHPCYGCNEEGIGFHKGIHQLAHVENQTPRSEKPDVNIKEGG.....NISAGAVG
EcHYB 225 GCKGPETYGNCSTLQFCDVGGVWPVAIGHPCYGCNEEGIGFHKGIHQLANVENQTPRSQKPDVNAKEGG.....NVSAGAIG
AvISP 220 GCKGPTTYNACATMKWND.GTSWPVEAGHPCLGCSEPQFWDAG..........G.FYEPVSVPLTLGP...ATLLGAGAA.
DvMSTD 221 GCKGPVTMNNCPKIKFNQ..TNWPVDAGHPCIGCSEPDFWDAM..........TPFYQN..................
DgSTD 218 GCKGPDTYNNCPKQLFNQ..VNWPVQAGHPCIACSEPNFWDLY..........SPFYSA..................
DdSTD 220 GCKGPETYNNCPKVLFNE..TNWPVAAGHPCIGCSEPNFWDDM..........TPFYQN..................
EcMBH 220 GCKGPTTYNACSSTRWND.GVSFPIQSGHGCLGCAENGFWDRG..........SFYSRVVDIPQMGTHSTADTVGLTALG
HmMBH 229 GCKGPTTYNACSTVRWNG.GTSFPIQSGHGCIGCSEDGFWDKG..........SFYSRDTEMNAFG.............
ReMBH 220 GCKGPTTYNACSTTRWNE.GTSFPIQSGHGCIGCSEDGFWDKG..........SFYDRLTGISQFGVEANADKIGGTASV
DvHSe 237 GCKGPMTMADCFERKWNG.GVNWCVQN.AVCIGCVEPDFPDGK..........SPFYQA..................
S77HYB 302 LLGGVVGLVAGVSVMAVRELGRQQKKDNADS....RGE...................
EcHYB 302 LLGGVVGLVAGVSVMAVRELGRQQKKDNADS....RGE...................
AvISP 285 ......GAVVGGGL...AALSRKKGRDAAAT....RQPVTVDELEQKL.........
DvMSTD ....
DgSTD ....
DdSTD ....
EcMBH 289 VVAAAVGVHAVASA.....VDQRRRHNQQPTETEHQPG.....NEDKQA........
HmMBH ....
ReMBH 289 VVGAAVTAHAAASA.....IKRASKKNETSG.SEHRSAWSHPQFEKRSAWSHPQFEK
DvHSe ....

B

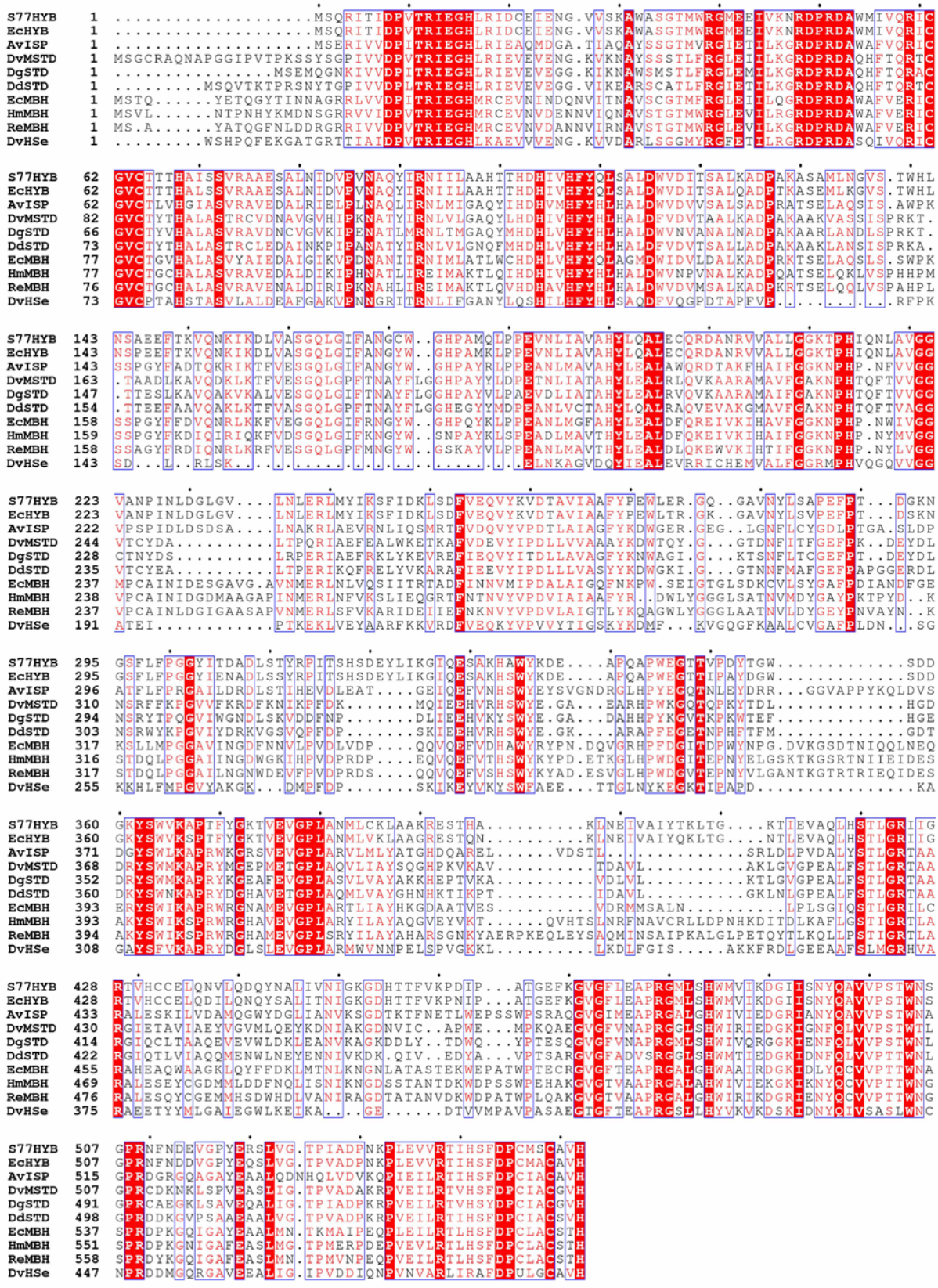
S77HYB
EcHYB
AvISP
DvMSTD
DgSTD
DdSTD
EcMBH
HmMBH
ReMBH
DvHSe

Fig. S6.

Amino acid sequence alignments of various [NiFe]-hydrogenases in Group 1. (A) Small subunits. (B) Large subunits. Residues with high degree of conservation are indicated in blue boxes, and strictly conserved residues are represented as white characters on a red background. The cysteine residues involved in the coordination to the proximal Fe-S cluster are marked with closed green circles. Two residues that would disturb a water relocation between the proximal cluster and water network around W1 (named as W1-net in S77HYB, see text) are marked with closed red circles. The residue that hydrogen bonds to W2 in S77HYB is marked with a closed cyan circle. Asp81 coordinated to Fe4 with a conformational change is marked with a closed blue circle. The sequences shown are the Hyb-type enzymes from *Citrobacter* sp. S-77 (S77HYB), and *E. coli* (EcHYB); the Isp-type enzyme from *Allochromatium vinosum* (AvISP); the STD-type enzymes from *Desulfovibrio vulgaris* Miyazaki F (DvMSTD), *Desulfovibrio gigas* (DgSTD), and *Desulfovibrio desulfuricans* (DdSTD); the MBH-type enzymes from *Hydrogenovibrio marinus* H110 (HmMBH), *Ralstonia eutropha* H16 (ReMBH), and *E. coli* (EcMBH); and the [NiFeSe]-hydrogenase from *D. vulgaris* Hildenborough (DvHSe).

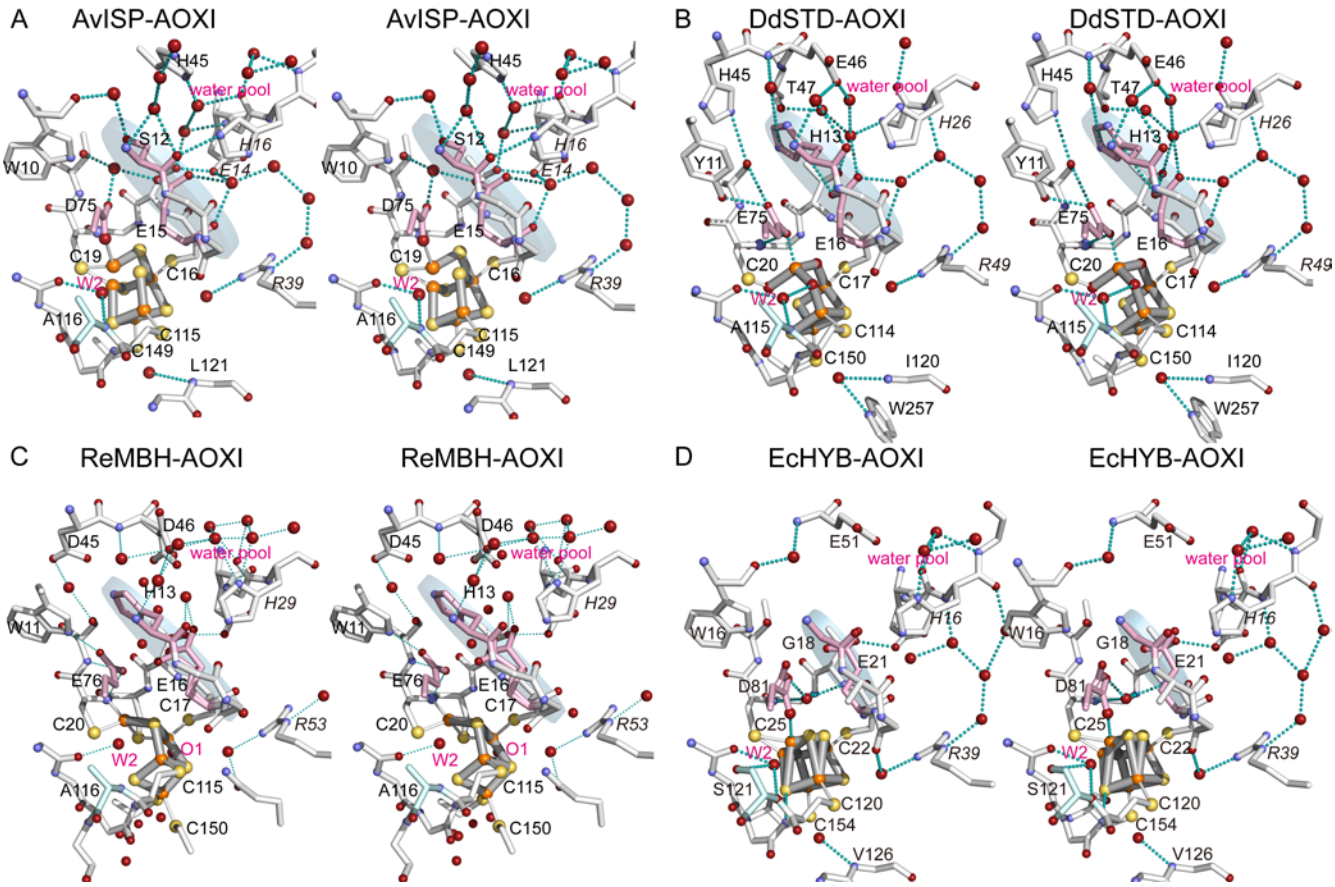

Fig. S7.

(**A, B, C, and D**) Stereo-views of the hydrogen-bonding networks around $[4Fe\text{-}4S]_P$ of AvISP (PDB ID: 3MYR), DdSTD (PDB ID: 1E3D), ReMBH (PDB ID:4IUB), and EcHYB (PDB ID:6EHQ) under AOXI, respectively. The "wall" (gray disc) formed by the loop region corresponds to -G18-T23- in S77HYB, and contains the bulky H13 in DdSTD and S12 (hydrogen-bonds to water molecules) in AvISP that may disturb the water molecule traffic between the water pool and $[4Fe\text{-}4S]_P$. O_2-tolerant ReMBH has a bulky H13 at this position, but probably uses another water escape route for O1. EcHYB has a small "wall" as in S77HYB, but A121 is replaced by S121 and its Oγ would disturb the flexibility of $[4Fe\text{-}4S]_P$ and the water molecule located at the corresponding position of W2 in S77HYB (labeled as W2). The residue names in the large subunit are labeled in italics. The atomic bonds of S12, E15, and D75 of AvISP; H13, E16, and D75 in DdSTD; H13, E16, and E76 in ReMBH; and G18, E21, and D81 in EcHYB are shown in pink, whereas those of A116 in AvISP; A115 in DdSTD; A116 in ReMBH, and S121 in EcHYB are shown in light cyan. $[4Fe\text{-}4S]_P$ is depicted by the thick bonds and possible hydrogen bonds are indicated by broken blue lines (atom colors: C, gray; N, blue; O, red; S, yellow; Fe, orange).

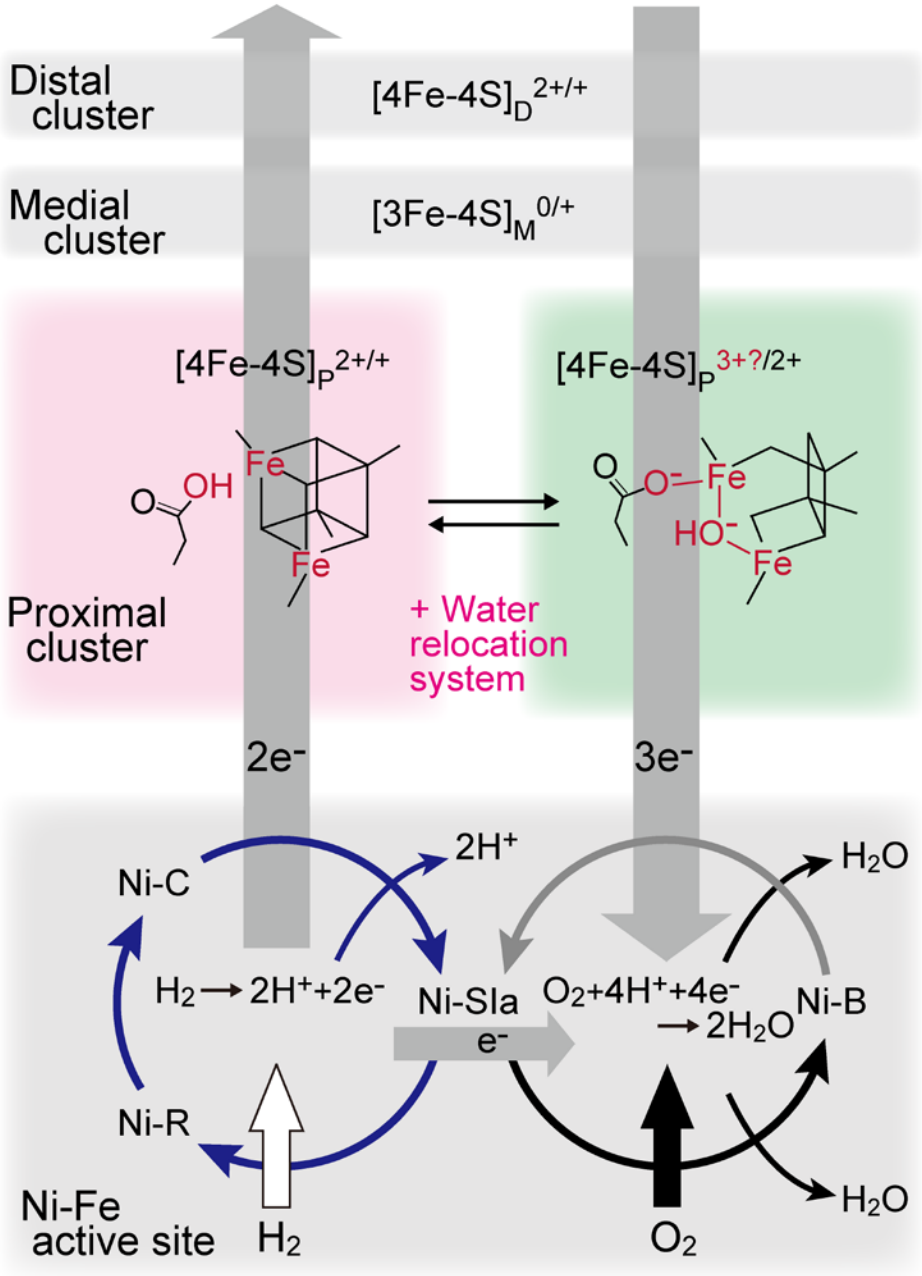

Fig. S8.

Molecular mechanism that protects the active site in S77HYB from O_2 damage. The upward thick gray arrow shows the electron flow of the H_2-uptake reaction from the active site to the clusters, whereas the downward and horizontal arrows show the back donation of the electrons from the clusters and Ni-SIa, respectively when the enzyme is oxidized. The pink and green backgrounds indicate the structures of the $[4Fe\text{-}4S]_P$ in the reduced and oxidized forms, respectively. To protect the active site from O_2 damage, $[4Fe\text{-}4S]_P$ in S77HYB supplies an additional electron being a deformed structure, and is stabilized by the negative charges of a nearby carboxylate and OH^-. These conformational changes are completely reversible with the concomitant relocation of water molecules.

SI Tables

Table S1A.

Crystal preparation conditions, x-ray data collection, and refinement statistics for [NiFe]-hydrogenase from *Citrobacter* sp. S-77 under various redox conditions

Data set	H_2-reduced	$K_3[Fe(CN)_6]$-oxidized	Air-oxidized
Preparation (gas condition)			
Purification	97%N_2+3%H_2	97%N_2+3%H_2	97%N_2+3%H_2
Crystallization	Aerobic	Aerobic	Aerobic
H_2-treatment	100% H_2	100% H_2	-
$K_3[Fe(CN)_6]$-treatment	-	100% N_2	-
Crystal parameter			
Space group	$P2_1$	$P2_1$	$P2_1$
Cell parameters *a, b, c* (Å)	65.73, 121.61, 98.88	65.97, 121.83, 99.17	63.94, 118.98, 96.81
β (°)	102.65	102.93	100.57
Data collection			
Wavelength (Å)	0.90000	0.90000	0.90000
Resolution range (Å) [a]	50.00-1.84 (1.89-1.84)	50.00-2.05 (2.10-2.05)	50.00-1.57 (1.58-1.57)
Total reflections	497642	363558	737813
Unique reflections	251118	184162	382238
R_{merge} [a, b]	5.8 (57.6)	8.3 (52.9)	6.9 (55.8)
Average $I/\sigma(I)$ [a, c]	11.3 (1.4)	10.9 (2.4)	7.3 (1.8)
Completeness [a]	96.8 (95.3)	97.5 (96.8)	97.5 (99.3)
Redundancy [a]	1.9 (1.9)	2.0 (2.0)	1.9 (1.9)
Refinement			
Resolution range (Å)	38.02-1.84	37.86-2.05	31.72-1.57
Total reflections	130761	94895	196578
R-factor/free *R*-factor [d, e]	0.180/0.219	0.166/0.217	0.122/0.166
Atoms in an asymmetric unit			
Protein	12678	12662	12838
Ligand	64	68	84
Solvent	525	522	1142
Deviation form ideal geometry			
Bond distances (Å)	0.010	0.010	0.008
Angle distances (Å)	1.438	1.328	1.302
Chiral volumes (Å^3)	0.099	0.093	0.074
Mean isotropic B-factors			
Main chain (Å^2)	22.2	13.7	17.5
Side chain (Å^2)	23.8	15.4	20.2
Ligand (Å^2)	22.6	12.6	17.4
Solvent (Å^2)	21.6	12.2	30.8
Ramachandran plot			
Favored	0.962	0.963	0.964
Allowed	0.035	0.036	0.035

Table S1B.
Re-refinement statistics for FOXI MBH-type [NiFe]-hydrogenases from *H. marinus*

Crystal parameter	
Space group	$P2_1$
Cell parameters	a = 75.63 Å, b = 116.94 Å, c = 113.34 Å, β = 91.42°
Refinement [f]	
Resolution range (Å)	20.00-1.32
Reflections/parameters	425556/147006
R-factor/free R-factor [d, e]	0.132/0.158
Atoms in an asymmetric unit	
Protein	14055
Ligand	90
Water	2189
Deviation form ideal geometry	
Bond distances (Å)	0.010
Angle distances (Å)	1.347
Chiral volumes (Å^3)	0.090
Mean isotropic B-factors	
Main chain (Å^2)	15.1
Side chain (Å^2)	17.7
Ligand (Å^2)	15.3
Water (Å^2)	35.4
Ramachandran plot	
Favored	0.973
Allowed	0.027

[a] Values in parentheses are for the highest resolution shells.
[b] R_{merge} = $\Sigma hkl\ \Sigma i(|Ii\ (hkl) - \langle I(hkl)\rangle|)/\Sigma hkl \Sigma i\ Ii(hkl)$.
[c] Signal-to-noise ratio of intensities.
[d] $R = \Sigma(|F_0 - F_C|)/\Sigma F_0$.
[e] To calculate the free R value, 5% of reflections were randomly chosen.
[f] Refinement was carried out for previously collected diffraction data (PDB ID:5Y34).

Table S2A.

Structural models and the resultant geometries obtained by geometry optimization.

Initial species given to U_B		U_A[a]	H_2O_A		HO_A^-		O_A^{2-}	
	H_2O_B	Structural model (charge, spin)	Model 1 (-2, 1/2)		Model 2 (-3, 1/2)		Model 3 (-4, 1/2)	
		Most stable spin state	BS34		BS34		BS34	
		Distances [b] [Å]	$HO_BH\ldots H—O_AH$		$HO_B—H\ldots O_AH$		$HO_B—H\ldots O_A$	
			$HO_BH\ldots H$	$H—O_AH$	$HO_B—H$	$H\ldots O_AH$	$HO_B—H$	$H\ldots O_A$
			1.50	1.03	1.13	1.63	1.05	1.44
		Deviation of U_A and U_B[b] [Å]	0.71	0.53	0.12	0.12	0.16	0.33
	HO_B^-	Structural model (charge, spin)	Model 7 (-3, 1/2)		Model 8 (-4, 1/2)		Model 9 (-5, 1/2)	
		Most stable spin state	BS34		BS23		BS23	
		Distances [b] [Å]	$HO_B—H\ldots O_AH$		$HO_B—H\ldots O_A$		$HO_B—H_N\ldots O_A$	
			$HO_B—H$	$H\ldots O_AH$	$HO_B—H$	$H\ldots O_A$	$HO_B—H_N$	$H_N\ldots O_A$
			0.99	1.61	1.03	1.48	1.02	3.40
		Deviation of U_A and U_B[b] [Å]	0.12	0.15	0.16	0.55	0.47	0.65

Table S2B

Structural models and the resultant geometries obtained by geometry optimization.

Initial species given to U_B		U_A[a]	O_A^-		HS_A^-		S_A^{2-}	
	H_2O_B	Structural model (charge, spin)	Model 4 (-3, 1)		Model 5 (-3, 1/2)		Model 6 (-4, 1/2)	
		Most stable spin state	BS23		BS34		BS12	
		Distances [b] [Å]	$HO_B—H\ldots O_A$		$HO_B—H\ldots S_AH$		$HO_B—H\ldots S_A$	
			$HO_B—H$	$H\ldots O_A$	$HO_B—H$	$H\ldots S_AH$	$HO_B—H$	$H\ldots S_A$
			1.01	1.55	0.98	1.99	0.99	2.12
		Deviation of U_A and U_B[b] [Å]	0.13	0.64	0.34	0.11	1.05	0.30
	HO_B^-	Structural model (charge, spin)	Model 10 (-4, 1)		Model 11 (-4, 1/2)		Model 12 (-5, 1/2)	
		Most stable spin state	BS23		BS34		BS12	
		Distances [b] [Å]	$HO_B—H_N\ldots O_A$		$HO_B—H_N\ldots S_AH$		$HO_B—H_N\ldots S_A$	
			$HO_B—H_N$	$H_N\ldots O_A$	$HO_B—H_N$	$H_N\ldots S_AH$	$HO_B—H_N$	$H_N\ldots S_A$
			1.05	3.70	1.03	3.65	1.03	3.40
		Deviation of U_A and U_B[b] [Å]	0.46	0.72	1.60	0.73	1.47	0.71